Modifying infrared scattering effects of single yeast cells with plasmonic metal mesh

Marvin A. Malone, Suraj Prakash, Joseph M. Heer, Lloyd D. Corwin, Katherine E. Cilwa, and James V. Coe[a)]

Department of Chemistry, The Ohio State University, 100 West 18th Avenue, Columbus, Ohio 43210-1173, USA

(Received 1 July 2010; accepted 4 October 2010; published online 8 November 2010)

The scattering effects in the infrared (IR) spectra of single, isolated bread yeast cells (*Saccharomyces cerevisiae*) on a ZnSe substrate and in metal microchannels have been probed by Fourier transform infrared imaging microspectroscopy. Absolute extinction $[(3.4 \pm 0.6) \times 10^{-7}$ cm^2 at 3178 cm$^{-1}]$, scattering, and absorption cross sections for a single yeast cell and a vibrational absorption spectrum have been determined by comparing it to the scattering properties of single, isolated, latex microspheres (polystyrene, 5.0 μm in diameter) on ZnSe, which are well modeled by the Mie scattering theory. Single yeast cells were then placed into the holes of the IR plasmonic mesh, i.e., metal films with arrays of subwavelength holes, yielding "scatter-free" IR absorption spectra, which have undistorted vibrational lineshapes and a rising generic IR absorption baseline. Absolute extinction, scattering, and absorption spectral profiles were determined for a single, ellipsoidal yeast cell to characterize the interplay of these effects. © *2010 American Institute of Physics*. [doi:10.1063/1.3505548]

I. INTRODUCTION

A single cell is the basic unit of eukaryotic microorganisms such as yeast. It is desirable to record infrared (IR) absorption spectra of single cells in order to assay the cell function or response to stimuli and insults[1–7] at this basic level of organization. However, cells are similar in size to the wavelength of IR light, which results in several problems including scattering that dominates vibrational features, distortion of vibrational lineshapes, and shifts of vibrational peak centers. The latter two effects are also known as the "dispersion artifact"[8] or the Christiansen effect.[9] Fourier transform infrared (FTIR) microscopes readily record signals from single cells, but the spectra are plagued by these well-documented scattering effects.[10–18] In this work, the scattering effects in single yeast cells are first characterized on a ZnSe substrate, and then individual cells are placed into the holes of the metal plasmonic mesh, which results in "scatter-free" IR absorption spectra. Heer *et al.*[19] previously demonstrated scattering reductions with 5 μm latex microspheres in mesh holes. Since much of the light is guided along the surface of the metal mesh by plasmonic mechanisms (like an "inside-out" fiber optic), microparticles within the holes experience evanescent light that is similar to the radiation that reaches just outside of an internally reflecting attenuated total reflection (ATR) crystal device. The "metal belt" around the microparticle must convert the trajectories that would be scattering in the absence of metal into guided light that is absorbed or transmitted. Observations on single yeast cells are combined on an absolute scale, which enables a sorting of scattering and absorption effects.

Baker's or bread yeast, *Saccharomyces cerevisiae*, is one of the simplest eukaryotic cells. The genome has been sequenced[20] and has 12 156 677 base pairs,[21] so the amount of DNA in each cell is precisely known. Bread yeast is much studied as it shares 23% (Ref. 22) of its genome with humans. While scattering is well understood for homogeneous spheres (by virtue of Mie Scattering theory—particularly the text by van de Hulst),[23,24] a yeast cell is approximately spheroidal (prolate ellipsoid) and inhomogeneous (central vacuole, small nucleus, and other organelles). It is interesting to see how the scattering of a yeast cell is both similar and different than that of the spherical Mie particles.

FTIR microspectroscopy has been used to discriminate related species in microbiology[25–27] and to follow the effects of external agents on cells.[28–30] There is much interest in using IR spectroscopy to characterize changes in cells upon transformations associated with cancer,[3,8,10,11,31–41] but cells (and some subcellular components) are about the same size as the probing IR wavelengths, which results in large scattering effects.[8,10–18] These effects must be avoided or controlled to make such investigations routine. Some progress has been made by Bassan *et al.*[8] in characterizing and correcting for Mie scattering effects by means of parametrized Kramers–Kronig transformations. Our strategy in this work is to avoid the scattering effects by enclosing the cell in a metal housing, which still transmits enough IR intensity by virtue of plasmonic effects.

The amide I band, which is a vibration involving the amide C=O bond in various protein structures, is a good example of the importance of scattering effects in the IR spectra. This band occurs in absorption at 1655 cm^{-1} in α-helix, 1628 cm^{-1} and 1683 cm^{-1} in β-sheet, 1672 cm^{-1} for turns, and 1642 cm^{-1} for random coils.[42] Fresh yeast cells have the amide I band at 1655 cm^{-1} as assayed with

[a)]Electronic mail: coe.1@osu.edu.

synchrotron FTIR indicating a dominance of α-helix; however, the peak shifts to 1625 cm^{-1} after an exposure to antimicrobial silver ions, which indicates β-sheet.[43] This study was performed on small clusters of yeast cells rather than individual yeast cells due to the large scattering effects of single, isolated cells that show a redshift of the amide I band. So the amide I band can be used to assay cell viability, but scattering is a big problem.

Yeast cells have a rather remarkable ability to dehydrate without dying, i.e., they undergo anhydrobiosis. They can survive almost complete dehydration and resume metabolic activity once water is reintroduced.[44,45] The disaccharide trehalose is thought to protect liposomes, cell membranes, and proteins from the ravages of dehydration. In fact, human fibroblast cells have been conferred the ability to withstand dessication by the introduction of *E. coli* genes for the expression of trehalose biosynthetic enzymes.[44] Initially, our work was set out to follow the IR spectral changes associated with the dessication of single yeast cells; however, it rapidly became evident that scattering was a big problem, which became the focus of this paper. The yeast cells in this work have had the external water removed, which maximizes the index of refraction in contrast to the background and enhances scattering effects. However, the process of internal dehydration was only just the beginning for all the cells studied in this work.

II. EXPERIMENTAL

Yeast cell samples were prepared by adding 2.0 mg of Fleischmann active dry yeast (from a local supermarket) to 200 ml distilled water at 38–48 °C, with incubation for approximately 10 min. A drop of this yeast solution was then placed on a substrate (either a 2 mm thick ZnSe window or a piece of plasmonic metal mesh), and it was allowed to evaporate. The ZnSe infrared window was only 50% transmitting, but that was sufficient to record extinction spectra. The plasmonic metal mesh, obtained from Precision Eforming (839 Route 13, Courtland, NY 13045, www.precision-eforming.com, Part No. MN47), is nickel with a square pattern of square holes. The mesh has a 12.6 μm hole-center to hole-center spacing (lattice parameter), a 5.0–5.5 μm hole width, and a thickness of ~2.0 μm. Light incident on the metal is not directly transmitted, but can still get through the hole by plasmonic mechanisms.[19,46–48] The yeast cells are about the same size as the Ni metal mesh holes, and the evaporation process causes the cells to be drawn into the holes of the mesh (probably by capillary forces). The spacing of the mesh holes primarily defines the accessible IR range, and the specific size of the holes must match the cells to be studied, so cells of other sizes would likely require noncommercial sources of mesh. To make absolute cross section measurements, the extinction spectra of yeast on ZnSe were compared to those of 5.0 μm latex microspheres [SPI Supplies, P.O. Box 656, West Chester, PA 19381-0656, www.2spi.com, Product No. 02705-AB, Lot No. 1120920, polystyrene, refractive index of 1.58 (at 540 nm), and a specified diameter of 5.0 ± 0.4 μm] on ZnSe, which are well modeled by the Mie scattering theory. Before describing the main subject of this work—the contrast of the IR spectra of single cells in mesh holes to the single cells on ZnSe—it was first necessary to carefully characterize the size and shape of the newly drying yeast cells.

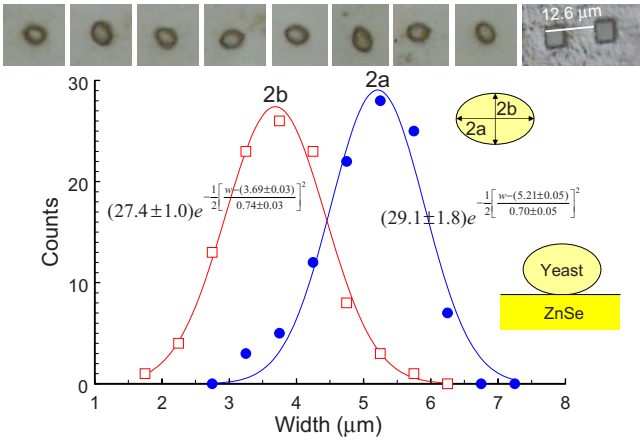

FIG. 1. Histograms of the lengths of the major and minor axes of single, isolated yeast cells on ZnSe, including nonlinear least-squares fits to Gaussian functions. At the top are a few selected optical microscope images of individual yeast cells from a set of 102 used to collect the histogram data.

Optical microscope images (Olympus BX40 with a 50× objective) of randomly selected yeast cells from a sample set of 102 single and isolated yeast cells on ZnSe are shown at the top of Fig. 1. An image of Ni mesh was obtained under the same conditions for calibration (see image at top right). The NIH freeware program, ImageJ, was used to draw a freehand line along the outside of each yeast cell image, which the program then fit to an ellipse. The program reported 2a (the long elliptical axis), 2b (the short elliptical axis), and the geometrical cross sectional area in units of pixels, which were converted to micron units by taking the average of the distance between several holes of the Ni mesh (12.6 μm lattice parameter, top right side of Fig. 1). Histograms of the major and minor ellipse axes were constructed with 0.5 μm bin widths. They were fit to Gaussian distributions as presented in Fig. 1. The best fit value of the long elliptical axis is $2a = 5.21 \pm 0.05$ μm and the short elliptical axis is $2b = 3.69 \pm 0.03$ μm, where the errors are estimated standard deviations in the mean. Since most of our intuition about scattering comes from spheres, the elliptical areas were also equated to the spherical area, yielding an effective spherical diameter of $2r_{eff} = 4.36 \pm 0.03$ μm or $r_{eff} = 2.18 \pm 0.02$ μm.

Infrared microspectroscopy studies of single isolated yeast cells were done in the imaging mode of a PerkinElmer Spectrum Spotlight 300 IR imaging microscope equipped with an array of 16 liquid-nitrogen-cooled mercury–cadmium–telluride detectors. The user defines a window region of the sample to study by drawing a rectangle over the area of interest in the optical microscope image. The microspectrometer records the full FTIR spectra at every position on a 6.25 μm square grid within the window. Typical experimental parameters were a range of 720–4000 cm^{-1} (up to 6000 cm^{-1} for some spectra of single yeast cells on ZnSe), a resolution of 4 cm^{-1}, 256 scans, and a nonpolarized light source. The system has a Cassegrain optical system

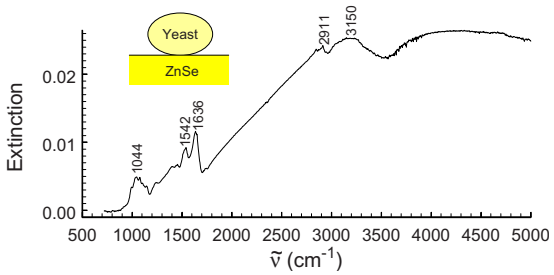

FIG. 2. Average IR extinction spectrum of 21 different, single, and isolated yeast cells on a ZnSe substrate. The effective window was 19.3 μm $\times$ 19.3 μm.

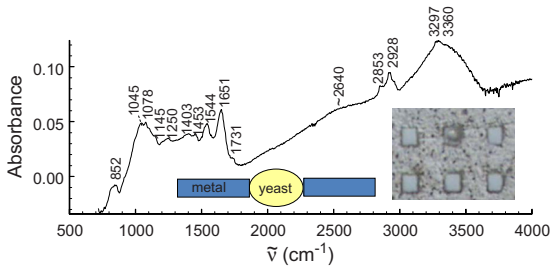

FIG. 3. Average IR absorption spectrum of 21 different, single, and isolated yeast cells in the holes of IR plasmonic metal mesh. The effective window was again 19.3 μm $\times$ 19.3 μm; however, this is strongly modified by the small fractional area of open mesh holes in the window.

such that the IR light impinges on the sample as a conical shell with a range of angles from 17° to 37° relative to the perpendicular of the sample surface. This disperses the plasmonic transmission resonances (as compared to a nonmicroscopic FTIR), greatly reducing the strength of plasmonic effects.

III. RESULTS

A. Volume of single yeast cell

Since the average yeast cell short axis (3.69 μm) is considerably shorter than the cell long axis (5.21 μm), it was presupposed that the cells will lay down on a short axis. Further, if the cells are assumed to be prolate ellipsoids (a better simplifying assumption than spherical), then the third axis (of length 2c) will be equal to 2b. The average volume per cell, $(4/3)\pi ab^2$, is 37.1 ± 1.4 μm^3 under these assumptions, which is a bit smaller than the volume obtained if the yeast cells are assumed to be spherical (43.4 μm^3).

B. Average spectra of single yeast cells on ZnSe

The average IR extinction spectrum of 21 different, single, and isolated yeast cells on ZnSe is shown in Fig. 2. Each contributing spectrum was measured with 256 scans using a detector curve background of a 50 μm $\times$ 50 μm empty region on the ZnSe. The spectrum of each cell was obtained by coadding the transmission spectra at each 6.25 μm grid point within a boxed region of 3 grid lengths by 3 grid lengths (18.75 μm $\times$ 18.75 μm), which collects light like an effective window of 19.3 μm $\times$ 19.3 μm. The coadded spectra of the cell were further ratioed to the coadded spectra within the same size empty box in a space adjacent to the cell. The resulting average spectrum is dominated by a broad scattering peak. Vibrations, particularly those at the scattering maximum, are distorted and shifted from their pure absorption positions.

C. Average spectra of single yeast cells in mesh holes

The average IR spectrum of 21 different, single, and isolated yeast cells in metal mesh holes is shown in Fig. 3. Each contributing spectrum was measured with 256 scans using a detector curve background of a 50 μm $\times$ 50 μm empty region on the Ni mesh—similar to the yeast on ZnSe data. Again, the spectrum of each cell in a mesh hole was obtained by coadding the transmission spectra at each grid point within a boxed region of 3 grid lengths (19.3 μm $\times$ 19.3 μm effective window). The coadded cell spectrum was further ratioed to the coadded spectrum within a similar size empty box in a space adjacent to the cell containing an empty hole. The absorptions are ~16 times larger in the mesh spectrum than on ZnSe because the mesh is plasmonic and the holes are only 16% of the microscope window. The resulting average spectrum has a gently rising background that is a characteristic of generic absorption and vibrational peaks that are not distorted by scattering. This behavior is the same as that observed in our studies of latex microspheres on ZnSe versus the microspheres in the holes of Ni micromesh.[19]

D. Absolute extinction cross sections

Extinction spectra were also recorded for single, isolated 5.0 μm diameter latex microspheres on ZnSe in order to calibrate our IR microspectrometer. They are expected to act like typical, homogeneous, spherical, dielectric particles, which are well treated by the Mie scattering theory. Some selected results on a single latex microsphere on ZnSe are compared to those of a single yeast cell on ZnSe in Fig. 4. Each particle has three traces, which correspond to three different square window sizes of edge 4, 5, and 6 grid lengths.

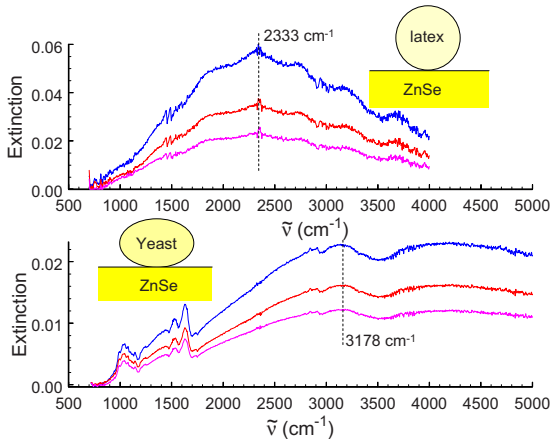

FIG. 4. Determination of the absolute extinction cross section of a yeast cell. Top: a set of extinction spectra for a single and isolated 5 μm latex sphere on ZnSe with windows of 4, 5, and 6 grid edges in length. Bottom: a set of extinction spectra for a single and isolated yeast cell on ZnSe with the same set of windows.

The problem is that the system has no real/physical aperture that defines the boxed region in which the spectra at the grid points are coadded. A square region of defined edge L exhibits an effective window size L_{eff} because the data are collected digitally rather than with a physical aperture. The known Mie scattering extinction cross section C_{ext} of a 5.0 μm diameter polystyrene microsphere is used to determine L_{eff} for any square boxed region chosen for analysis. The measured transmittance (t), or extinction (E), and L_{eff} are related to the extinction cross section by

$$C_{\text{ext}} = L_{\text{eff}}^2(1-t) = L_{\text{eff}}^2(1-10^{-E}). \tag{1}$$

Lumerical's finite difference time domain program was checked by reproducing calculations on dielectric spheres and then was used to calculate extinction as a function of wavelength using a spherical particle with a radius of 2.50 μm and an index of refraction of 1.58 on a flat substrate with an index of refraction of 2.40 (for ZnSe). The value of the extinction cross section at the maximum was $C_{\text{ext}}=8.54\times10^{-7}$ cm^2, which corresponds to a value of $Q_{\text{ext}}=4.35$ in the dimensionless units of the cross section divided by the area of the spherical particle, $Q_{\text{ext}}=C_{\text{ext}}/(\pi r^2)$. This calibrating extinction cross section was used with the transmission measurements at the maximum of scattered intensity and Eq. (1) for the boxed regions of lengths 4, 5, and 6 grid lengths (25.00, 31.25, and 37.50 μm), yielding values of $L_{\text{eff}}=26.68$, 33.75, and 41.21 μm, respectively. So the actual instrumental windows were only a small fraction of the grid width larger than expected. The same size windows and their calibrated L_{eff} sizes were used to determine the extinction cross section of three different yeast cells, yielding cross sections at maximum scattering at 3178 cm^{-1} of $(3.00\pm0.25)\times10^{-7}$ cm^2, $(4.1\pm0.5)\times10^{-7}$ cm^2, and $(3.00\pm0.18)\times10^{-7}$ cm^2. This corresponds to an average value for the extinction cross section of a single isolated yeast cell of $(3.4\pm0.6)\times10^{-7}$ cm^2 at the intensity maximum.

E. Common absolute plot of extinction, scattering, and absorption for a single, average yeast cell

The absolute maximum extinction cross section of 3.4×10^{-7} cm^2 fixed the scaling of the extinction spectrum, which was important because it was independent of any models. All remaining scaling and offsets were set by applying a full Mie model for a spherical particle including vibrations. The constraint was that a single set of parameters should reasonably represent all three absolute spectra for extinction, scattering, and absorption. The experimental extinction spectrum required only an offset from the Mie model as scaling was independently set. Since extinction (or scattering or absorption) spectra must monotonically decrease to zero as wavenumbers approach zero, the dip of the spectrum in Fig. 2 to about zero at 700 cm^{-1} shows that a positive offset was needed. Both offset and scaling are required to place the mesh absorption spectrum of Fig. 3 onto the absolute scale (dip below zero shows that a significant positive offset was needed). Since scattering is the difference between extinction and absorption, a second important constraint arises by subtracting the scaled and offset experimental extinction and absorption spectra to get an absolute scattering spectrum. The intensity and lineshape of each vibrational band in the absolute extinction, scattering, and absorption spectra were required to be consistent with a single set of Lorentz vibrational parameters.

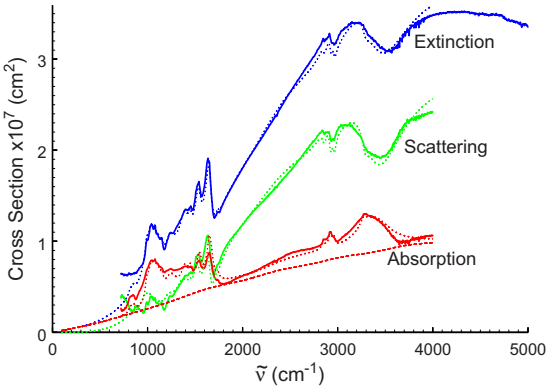

FIG. 5. Absolute cross section for extinction, scattering, and absorption of a single, average, newly dried, yeast cell on ZnSe. The dotted traces are Mie model simulations. The dashed curve is the vibrationless Mie model curve for absorption.

Cross sections were calculated numerically using the full Mie theory by calculating well-known a_n and b_n coefficients, given the complex index of refraction of the particle (m) and the particle radius (r) as described extensively by van de Hulst.[23] Vibrations are included as a sum term with the complex dielectric function (ϵ), which when written in terms of the index of refraction (m) is

$$m^* = \sqrt{\epsilon} = \sqrt{\epsilon' + i\epsilon'' + \sum_j \frac{A_j\tilde{\nu}_{0j}^2}{\tilde{\nu}_{0j}^2 - \tilde{\nu}^2 - \gamma\tilde{\nu}}}, \tag{2}$$

where m^* is the complex conjugate of m, ϵ' is the real constant part of ϵ, ϵ'' is the imaginary constant part of ϵ, and j is an index for a sum over vibrations (A_j is the strength, $\tilde{\nu}_{0j}$ is the position, and γ_j is the full width at half maximum of each vibration). The extinction (C_{ext}), scattering (C_{sca}), and absorption (C_{abs}) cross sections are calculated in the standard way with Mie theory

$$C_{\text{ext}} = \frac{1}{2\pi\tilde{\nu}^2}\sum_{n=1}^{\infty}(2n+1)[\text{Re}(a_n+b_n)], \tag{3}$$

$$C_{\text{sca}} = \frac{1}{2\pi\tilde{\nu}^2}\sum_{n=1}^{\infty}(2n+1)[|a_n|^2+|b_n|^2], \tag{4}$$

where $C_{\text{abs}}=C_{\text{ext}}-C_{\text{sca}}$. Truncation of the infinite sums at $n=20$ was sufficient for this project. The resulting absolute extinction, scattering, and absorption spectra are shown in Fig. 5 (absolute scaled experimental spectra are shown with solid traces). The model involved the following parameters: an offset of 0.0060 was added to the extinction spectrum of Fig. 2, which was multiplied by a factor of 1.086×10^{-5} to give the desired absolute maximum intensity. The experimental mesh absorption spectrum of Fig. 3 was offset by 0.068 and multiplied by $1.086\times10^{-5}/16$, so the mesh absorption is about 16 times stronger than would be expected

TABLE I. Lorentz vibrational parameters.

A_j	$\tilde{\nu}_{0j}$ (cm^{-1})	γ_j (cm^{-1})
0.017	3390	370
0.001 3	3278	80
0.000 40	2961	30
0.000 85	2922	40
0.000 40	2850	45
0.010	2630	810
0.000 4	2000	200
0.000 4	1742	30
0.011	1654	60
0.007 5	1544	65
0.002 0	1454	40
0.010	1395	100
0.017	1245	150
0.003 5	1149	40
0.006	1110	50
0.003 0	1080	30
0.029	1040	90
0.004 2	992	35
0.002 5	854	40
0.002 5	820	40

with a cell on ZnSe and no mesh. The Mie parameters were $r=1.94$ μm, $\epsilon'=1.843$, and $\epsilon''=0.170$ (in terms of the constant part of $m=n-ik$, $n=1.359$, and $k=0.063$). The vibrational parameters defined in Eq. (2) are given in Table I. Only 20 terms were used, so this model involves some shortcuts (using one term for many vibrations, particularly in the molecular finger print region). Once elliptical particles are sufficiently different than spherical particles, it will not be possible to correctly predict both the absolute intensity and the broad spectral lineshape with a spherical model. The simulation of Fig. 5 is reasonable, but less than ideal, and the parameters in Table I might change with a better model. Finally, by not including the terms in Table I, one obtains a vibrationless curve for the absolute absorption cross section (dashed curve), which was used to provide a more in depth analysis of the vibrational spectrum.

F. Reconstruction and fit of the vibrational absorption spectrum of a single yeast cell

The vibrationless curve was subtracted from the absolute absorption spectrum in Fig. 5 and then rescaled (divided by 1.086×10^{-5}) to obtain the vibrational absorption spectrum that would have been obtained by a single yeast cell on ZnSe if it did not scatter and was obtained under the same conditions as the extinction spectrum, as shown in Fig. 6. The vibrational peaks were fit to Gaussians in several ways as summarized in Table II, which includes assignments, peak positions, intensities, full width at half maximum, and integrated area. It was difficult to get definitive fits below the amide I band due to the large density of vibrations in the fingerprint region, so most entries at lower wavenumbers than the amide I band are not fitted positions, rather peak

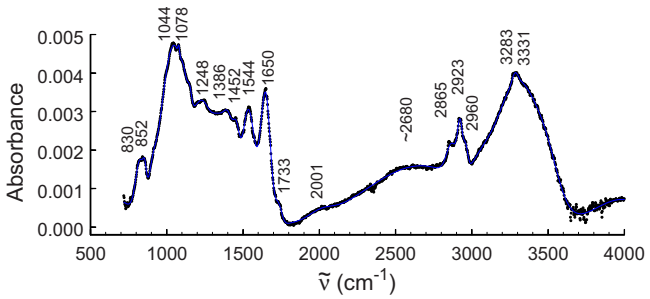

FIG. 6. IR vibrational absorption of an average single yeast cell as if it were on a ZnSe substrate with a 19.3 μm$\times$19.3 μm window with generic absorption subtracted away. The results of a nonlinear least-squares fitting (dotted line) of the peaks are given in Table II.

maxima. The H-bonded, OH stretching feature was fit with both one and three peaks to support alternative interpretations.

IV. DISCUSSION

Single, isolated, ellipsoidal yeast cells on ZnSe have extinction spectra that are dominated by scattering. They exhibit a very broad peak with a maximum near the nominal size of the cell, which is similar to the Mie scattering of spherical particles. There is the distortion of the vibrational lineshapes, particularly for the CH and OH stretches that are near the scattering maximum, but also at the amide I band. These scattering effects are greatly reduced by placing a yeast cell in the microhole of the plasmonic metal mesh. It

TABLE II. Vibrations of a single, average, newly dried yeast cell in absorption (spectrum in Fig. 6) with an effective window that is 19.3 μm $\times$19.3 μm. Peaks without the fit parameters are unfitted peak maxima. The ? symbol indicates assignments that are uncertain.

Vibration	$\tilde{\nu}$ (cm^{-1})	Intensity (absolute units)	Int. area (cm^{-1})	FWHM (cm^{-1})
OH stretch 1	3331	0.003 65	1.574	405
OH stretch 3	3497	0.000 89	0.180	189
	3306	0.003 39	1.178	326
	3060	0.000 43	0.076	166
NH stretch	3284	0.000 24	0.0107	42
CH_3 stretch	2960	0.000 59	0.021	33
CH_2 a stretch	2924	0.001 18	0.048	38
CH_2 s stretch	2870	0.000 77	0.065	80
Scat. peak?	2668	0.001 60	1.469	865
H_2O ν_2+lib.	2011	0.000 17	0.031	178
C=O	1734	0.000 47	0.024	48
	1732			
Amide I	1649	0.003 35	0.270	76
	1650			
Amide II	1536	0.003 03	0.339	105
	1544			
CH_2 bend	1452			
$C(CH_3)_2$ str?	1402			
PO_2^{2-} asym	1248			
Carbohyd.?	1142			
PO_2^{2-} sym	1078			
Glucans?	1044			
Glyco. link?	852			
Mannans?	830			

becomes possible to characterize a single yeast cell absorption spectrum without the phasing distortions brought on by the interaction of scattered light with vibrations.

The challenge emerged to place the extinction spectrum and absorption spectrum of a single yeast cell onto the same common and absolute scale, while being mindful of plasmonic effects or distortions. Individual latex microspheres work very nicely to calibrate the effective window of the imaging FTIR microspectrometer; however, the required offsets add systematic uncertainty to the absolute results. Examination of the low wavenumber region of the extinction spectrum in Fig. 2 (which is close to zero intensity at 700–800 cm^{-1}) and knowledge about trends (intensity monotonically decreases to zero at zero wavenumbers) argues for a positive offset. An offset was also required for the absorption spectrum of Fig. 3 before scaling. Examination of Fig. 3 reveals an absorbance of -0.03 at ~ 700 cm^{-1}, while the trends in generic absorption require this value to be positive. This offset likely comes from the imperfect subtraction of dispersed plasmonic resonances with and without the particle of interest in the holes. The only constraint on these offsets was the internal consistency of the extinction, scattering, and absorption curves in Fig. 5 which was not quantified. Consequently, there could be systematic errors in the absolute cross sections at the level of 30%, which go with random variations of $\sim 18\%$.

It is interesting to consider the differences of water within the average, single yeast cell to bulk liquid water. The OH stretching band of a yeast cell (Fig. 6) is less wide (FWHM=405 cm^{-1}) than in liquid water and occurs at a fitted value of 3331 cm^{-1}, which is significantly red shifted from the pure liquid water value[49] of 3404 cm^{-1}. It is well known that water molecules bind more tightly to cellular biomolecules than they do to each other in bulk water.[50] This produces an icelike redshift in the OH stretching frequency. By the same analogy, one also expects an increase in the intensity for a given amount of water.

The water inside an average, freshly dried, single yeast cell produces an OH stretch absorption signal with a cross section of 5.5×10^{-8} cm^2 at 3346 cm^{-1}. A crude estimate of the water in a single yeast cell (assuming that the cell volume of 37.1 μm^3 is 75% water[51]) yields ~ 27.9 pg or $\sim 1.55\times10^{-12}$ moles. According to the Mie model simulation, this amount of water produces an absorbance of 0.003 65 when assayed with a 19.3 $\mu m\times 19.3$ μm window. The vibrational parameter $A_{OH}=0.017$ for the OH stretch of water in a single yeast cell also provides an alternative measure of the strength of the OH absorption within a Mie modeling context using dielectric functions.

The OH peak in liquid water is well-known for an extensive red tail associated with hydrogen bonding. In the extinction spectra of a single yeast cell (see Fig. 2), the OH band seems to stretch all the way down to the fingerprint region at ~ 1700 cm^{-1}. However, examination of Fig. 6 shows that this long tail is due to several effects not associated with OH stretching, including a broad feature that might be due to residual scattering at ~ 2680 cm^{-1} and the ν_2 +libration combination band of water. Concerning the latter, the H_2O ν_2+libration feature[49] will have an intensity of 3% of the OH stretch in liquid water predicting an absorbance of 0.000 11, while we see 0.000 17. Concerning the possible residual scattering feature, it may be that the suppression of scattering from the full cell shape leaves residual scattering effects from some of the internal structures such as the nucleus or central vacuole. Scattering in this region has been observed from pycnotic (inactive and contracted) nuclei of human cells.[14] Recalling that Fig. 6 is an average spectrum of many individuals, note that the individual spectra show variations in the position and width of this feature including some spectra without this feature. Therefore, more work is needed before a definitive assignment can be offered.

The removal of scattering effects in Fig. 6 reveals a smaller and less broad peak on top of the OH stretching band. The nonlinear least-squares fitting reveals this peak to be at 3283 cm^{-1} with a full width at half maximum (FWHM) of 42 cm^{-1}. Stretching of the NH group in both proteins and peptides occurs in this region (3300 and 3080 cm^{-1}), respectively,[52] which is usually obscured by the large OH stretching band.

The peak at 1248 cm^{-1} is attributed to nucleic acids and is of much interest since a diploid bread yeast cell will have 0.024 pg of DNA. However, there may be as much as 100 times more RNA than DNA in a functional yeast cell,[51] so it is thought that this peak is much more likely to characterize RNA. Clearly, there exists the potential to quantify the amount of RNA in a single yeast cell.

The amide I band, which is diagnostic of the viability of cells,[42] is significantly affected by scattering although these effects are not as apparent as with the OH and CH stretching vibrations that occur closer to the scattering maximum. The amide I band has significant derivative character in the extinction spectrum and the upward part of the lineshape occurs at 1636 cm^{-1}. If this were interpreted as an absorption, the feature would suggest a significant change from the dominance of α-helix structure at 1655 cm^{-1}, perhaps suggesting cell death. However, the position of the amide I band maximum at 1650 cm^{-1} in the absorption-corrected spectrum of Fig. 6 suggests that the yeast cells are alive and well.

V. CONCLUSION

In yeast cells, there exists an interesting interplay between scattering, vibrations, and generic absorption. The generic absorption and scattering curves cross over from the dominance of scattering to absorption at wavenumbers lower than 1800 cm^{-1}, which is right in the middle of a traditional IR spectrum. Both dramatic and subtle scattering effects were revealed, which importantly affect the interpretation of observed IR spectra of single yeast cells.

ACKNOWLEDGMENTS

We thank the National Science Foundation for the support of this work under Grant Nos. CHE 0848486 and CHE-0639163.

[1] M. Harz, P. Rosch, and J. Popp, Cytometry, Part A **75A**, 104 (2009).
[2] M. Diem, L. Chiriboga, P. Lasch, and A. Pacifico, Biopolymers **67**, 349 (2002).
[3] M. Romeo, C. Matthäus, M. Miljkovic, and M. Diem, Biopolymers **74**,

168 (2004).
[4] M. Miljkovic, M. Romeo, C. Matthäus, and M. Diem, Biopolymers **74**, 172 (2004).
[5] M. J. Tobin, L. Puskar, R. L. Barber, E. C. Harvey, P. Heraud, B. R. Wood, K. R. Bambery, C. T. Dillon, and K. L. Munro, Vib. Spectrosc. **53**, 34 (2010).
[6] N. Jamin, P. Dumas, J. Moncuit, W.-H. Fridman, J.-L. Teillaud, G. L. Carr, and G. P. Williams, Proc. Natl. Acad. Sci. U.S.A. **95**, 4837 (1998).
[7] P. Lasch, M. Boese, A. Pacifico, and M. Diem, Vib. Spectrosc. **28**, 147 (2002).
[8] P. Bassan, A. Kohler, H. Martens, J. Lee, H. J. Byrne, P. Dumas, E. Gazi, M. Brown, N. Clarke, and P. Gardner, Analyst (Cambridge, U.K.) **135**, 268 (2010).
[9] C. Christiansen, Ann. Phys. **259**, 298 (1884).
[10] P. Bassan, H. J. Byrne, F. Bonnier, J. Lee, P. Dumas, and P. Gardner, Analyst (Cambridge, U.K.) **134**, 1586 (2009a).
[11] P. Bassan, H. J. Byrne, J. Lee, F. Bonnier, C. Clarke, P. Dumas, E. Gazi, M. D. Brown, N. W. Clarke, and P. Gardner, Analyst (Cambridge, U.K.) **134**, 1171 (2009b).
[12] A. Kohler, J. Sulé-Suso, G. D. Sockalingum, M. Tobin, F. Bahrami, Y. Yang, J. Pijanka, P. Dumas, M. Cotte, D. G. van Pittius, G. Parkes, and H. Martens, Appl. Spectrosc. **62**, 259 (2008).
[13] J. Lee, E. Gazi, J. Dwyer, M. D. Brown, N. W. Clarke, J. M. Nicholson, and P. Gardner, Analyst (Cambridge, U.K.) **132**, 750 (2007).
[14] B. Mohlenhoff, M. Romeo, M. Diem, and B. R. Wood, Biophys. J. **88**, 3635 (2005).
[15] J. K. Pijanka, A. Kohler, Y. Yang, P. Dumas, S. Chio-Srichan, M. Manfait, G. D. Sockalingum, and J. Sulè-Suso, Analyst (Cambridge, U.K.) **134**, 1176 (2009).
[16] M. Romeo and M. Diem, Vib. Spectrosc. **38**, 129 (2005).
[17] M. Romeo, B. Mohlenhoff, and M. Diem, Vib. Spectrosc. **42**, 9 (2006).
[18] S. Boydston-White, T. Gopen, S. Houser, J. Bargonetti, and M. Diem, Biospectroscopy **5**, 219 (1999).
[19] J. Heer, L. Corwin, K. Cilwa, M. A. Malone, and J. V. Coe, J. Phys. Chem. C **114**, 520 (2010).
[20] N. Williams, Science **272**, 481 (1996).
[21] P. Lefrancois, G. Euskirchen, R. Auerbach, J. Rozowsky, T. Gibson, C. Yellman, M. Gerstein, and M. Snyder, BMC Genomics **10**, 37 (2009).
[22] International Human Genome Sequencing Consortium E. S. Lander *et al.* , Nature (London) **409**, 860 (2001).
[23] H. C. van de Hulst, *Light Scattering by Small Particles* (Dover, New York, 1981).
[24] M. Mishchenko, *Scattering, Absorption, and Emission of Light by Small Particles* (Cambridge University Press, Cambridge, 2002).
[25] L. Mariey, J. P. Signolle, C. Amiel, and J. Travert, Vib. Spectrosc. **26**, 151 (2001).
[26] N. A. Ngo-Thi, C. Kirschner, and D. Naumann, J. Mol. Struct. **661**, 371 (2003).
[27] M. Wenning, H. Seiler, and S. Scherer, Appl. Environ. Microbiol. **68**, 4717 (2002).
[28] P. Dumas, N. Jamin, J. Teillaud, M. Miller, and B. Beccard, Faraday Discuss. **126**, 289 (2004).
[29] H.-Y. N. Holman, R. Goth-Goldstein, M. C. Martin, M. L. Russell, and W. R. McKinney, Environ. Sci. Technol. **34**, 2513 (2000).
[30] J. Sulé-Suso, D. Skingsley, G. D. Sockalingum, A. Kohler, G. Kegelaer, M. Manfait, and A. J. El Haj, Vib. Spectrosc. **38**, 179 (2005).
[31] M. Diem, M. Romeo, C. Matthäus, M. Miljkovic, L. Miller, and P. Lasch, Infrared Phys. Technol. **45**, 331 (2004).
[32] E. Gazi, J. Dwyer, N. P. Lockyer, J. Miyan, P. Gardner, C. A. Hart, M. D. Brown, and N. W. Clarke, Vib. Spectrosc. **38**, 193 (2005).
[33] M. J. German, A. Hammiche, N. Ragavan, M. J. Tobin, L. J. Cooper, S. S. Matanhelia, A. C. Hindley, C. M. Nicholson, N. J. Fullwood, H. M. Pollock, and F. L. Martin, Biophys. J. **90**, 3783 (2006).
[34] D. A. Moss, M. Keese, and R. Pepperkok, Vib. Spectrosc. **38**, 185 (2005).
[35] M. J. Tobin, M. A. Chesters, J. M. Chalmers, F. J. M. Rutten, S. E. Fisher, I. M. Symonds, A. Hitchcock, R. Allibone, and S. Dias-Gunasekara, Faraday Discuss. **126**, 27 (2004).
[36] R. Bhargava, Anal. Bioanal. Chem. **389**, 1155 (2007).
[37] B. Bird, BMC Clin. Pathol. **8**, 8 (2008).
[38] R. K.Dukor, J. M. Chalmers, and P. R. Griffiths, *Handbook of Vibrational Spectroscopy* (Wiley, New York, 2001), Vol. 5, p. 3335.
[39] D. C. Fernandez, R. Bhargava, S. M. Hewitt, and I. W. Levin, Nat. Biotechnol. **23**, 469 (2005).
[40] E. Gazi, M. Baker, J. Dwyer, N. P. Lockyer, P. Gardner, J. H. Shanks, R. S. Reeve, C. A. Hart, N. W. Clarke, and M. D. Brown, Eur. Urol. **50**, 750 (2006).
[41] B. R. Wood, L. Chiriboga, H. Yee, M. A. Quinn, D. McNaughton, and M. Diem, Gynecol. Oncol. **93**, 59 (2004).
[42] A. Barth and C. Zscherp, Q. Rev. Biophys. **35**, 369 (2002).
[43] C. Saulou, F. Jamme, C. Maranges, I. Fourquaux, B. Despax, P. Raynaud, P. Dumas, and M. Mercier-Bonin, Anal. Bioanal. Chem. **396**, 1441 (2010).
[44] N. Guo, I. Puhlev, D. R. Brown, J. Mansbridge, and F. Levine, Nat. Biotechnol. **18**, 168 (2000).
[45] S. B. Leslie, Appl. Environ. Microbiol. **61**, 3592 (1995).
[46] J. V. Coe, J. M. Heer, S. Teeters-Kennedy, H. Tian, and K. R. Rodriguez, Annu. Rev. Phys. Chem. **59**, 179 (2008).
[47] J. V. Coe, K. R. Rodriguez, S. Teeters-Kennedy, K. Cilwa, J. Heer, H. Tian, and S. M. Williams, J. Phys. Chem. C **111**, 17459 (2007).
[48] K. E. Cilwa, K. R. Rodriguez, J. M. Heer, M. A. Malone, L. D. Corwin, and J. V. Coe, J. Chem. Phys. **131**, 061101 (2009).
[49] J.-J. Max and C. Chapados, J. Chem. Phys. **131**, 184505 (2009).
[50] P. Nicholls, Cell. Mol. Life Sci. **57**, 987 (2000).
[51] F. Sherman, Methods Enzymol. **350**, 3 (2002).
[52] E. Burattini, M. Cavagna, R. Dell'Anna, F. Malvezzi Campeggi, F. Monti, F. Rossi, and S. Torriani, Vib. Spectrosc. **47**, 139 (2008).